Improving Global Model Precipitation Forecasts over India Using Downscaling and the FSU Superensemble. Part II: Seasonal Climate

ARINDAM CHAKRABORTY* AND T. N. KRISHNAMURTI

Department of Meteorology, The Florida State University, Tallahassee, Florida

(Manuscript received 25 July 2008, in final form 9 December 2008)

ABSTRACT

This study addresses seasonal forecasts of rains over India using the following components: high-resolution rain gauge–based rainfall data covering the years 1987–2001, rain-rate initialization, four global atmosphere–ocean coupled models, a regional downscaling of the multimodel forecasts, and a multimodel superensemble that includes a training and a forecast phase at the high resolution over the internal India domain. The results of monthly and seasonal forecasts of rains for the member models and for the superensemble are presented here. The main findings, assessed via the use of RMS error, anomaly correlation, equitable threat score, and ranked probability skill score, are (i) high forecast skills for the downscaled superensemble-based seasonal forecasts compared to the forecasts from the direct use of large-scale model forecasts were possible; (ii) very high scores for rainfall forecasts have been noted separately for dry and wet years, for different regions over India and especially for heavier rains in excess of 15 mm day^{-1}; and (iii) the superensemble forecast skills exceed that of the benchmark observed climatology. The availability of reliable measures of high-resolution rain gauge–based rainfall was central for this study. Overall, the proposed algorithms, added together, show very promising results for the prediction of monsoon rains on the seasonal time scale.

1. Introduction

Prediction of the seasonal climate of the Asian monsoon has been a challenging scientific problem. Gilbert Walker's (Walker 1923, 1924) pioneering works were the first studies on the ENSO–monsoon relationship. In those studies, a higher- or lower-than-normal sea level pressure over the western equatorial Pacific was used to assess the monsoon rains of a subsequent season over India. Over the last 20 yr many efforts have been made on the seasonal climate forecasts of the Asian summer monsoon. These are referenced in the special volumes on monsoon meteorology by Chang and Krishnamurti (1987), Chang (2004), Chang et al. (2005), Wang (2006), and others. This progress has been in three areas of research that include statistical extensions of Gilbert Walker's work, dynamical modeling, and in the area of combined dynamical–statistical modeling.

The India Meteorological Department (IMD) has used multiple preseason statistical predictors to provide seasonal forecasts of the Indian summer monsoon rainfall (Gowariker et al. 1991; Thapliyal and Kulshrestha 1992; Rajeevan et al. 2004, and others). These studies utilized parameters such as Eurasian snow cover, the Niño-3 SST anomaly, the Europe pressure gradient, the South Indian Ocean SST index, etc., as predictors. The primary goal of these multipredictor statistical models is to forecast the seasonal mean monsoon rainfall averaged over the Indian region.

Current dynamical models involve monsoon forecasts from coupled atmosphere–ocean global climate models (Yang and Anderson 2000; Krishnamurti et al. 2002; Palmer et al. 2004; Kumar et al. 2005; Wang et al. 2005; Krishnamurti et al. 2006b, and others). Some improved seasonal forecasts by the dynamical method have been possible from the use of a suite of multiple forecasts. These were based either for single models (utilizing multiple initial conditions) or from the use of multimodel (Peng et al. 2002; Palmer et al. 2004; Krishnamurti et al. 2006a; Chakraborty and Krishnamurti 2006). Statistical postprocessing of seasonal monsoon forecasts from multimodels utilizing approaches like ensemble mean, superensemble, and from other cluster averaging have

* Current affiliation: Centre for Atmospheric and Oceanic Sciences, Indian Institute of Science, Bangalore, India.

Corresponding author address: Arindam Chakraborty, Department of Meteorology, The Florida State University, Tallahassee, FL 32306. E-mail: arch@io.met.fsu.edu

DOI: 10.1175/2009MWR2736.1

defined the current state of art in this area. These statistical–dynamical combinations have provided improvements over those possible for the use of single atmosphere–ocean coupled climate models (Brankovic et al. 1990; Brankovic and Palmer 1997; Sperber and Palmer 1996; Stephenson et al. 2005). The horizontal resolution used in most of these models has generally been of the order of 100–250 km. This had the limitation for predicting the regional climate needed for the provinces of India (Gadgil and Kumar 2006).

Categorical forecasts using ensemble of simulations (either from a single model with multiple initial condition or from multiple models) is one approach for forecasting extreme events. Rajagopalan et al. (2002) used this approach to forecast precipitation and temperature over the globe on a seasonal time scale. Regonda et al. (2006) initiated a new approach for categorical streamflow forecast using leading modes of principle components of the flow and large-scale climate variables. Logistic regression between different parameters is another approach for forecasting extreme events (e.g., Hamill et al. 2004).

Higher-resolution forecasts of monsoon climate can be approached from the direct use of a suite of mesoscale models (Ji and Vernekar 1997; Vernekar and Ji 1999) or from the deployment of downscaling strategies (e.g., Misra and Kanamitsu 2004; Tripathi et al. 2006; Anandhi et al. 2008). A direct use of observed high-resolution precipitation estimates is possible in the context of downscaling for coupled climate modeling. This is the main objective of this study. Krishnamurti et al. (2009, hereafter Part I) used a suite of atmospheric models for medium-range numerical weather prediction. In this study we propose a two-step approach for the prediction of monthly to seasonal monsoon precipitation in a regional scale over the Indian domain. At first, a downscaling strategy is used to obtain precipitation forecasts from coupled climate models at the resolution of a new rain gauge–based dataset. The next step is to use the superensemble methodology (Krishnamurti et al. 1999) to construct a consensus forecast from these downscaled model forecasts that usually provides higher skills than the individual member models and their ensemble mean for seasonal climate prediction (Krishnamurti et al. 2000b; Stefanova and Krishnamurti 2002; Chakraborty and Krishnamurti 2006). The next section describes the models and datasets used in this study. The downscaling strategy is detailed in section 3. The superensemble methodology and the coupled assimilation procedure are described in sections 4 and 5, respectively. Section 6 outlines the seasonal forecast experiments. The results are illustrated in section 7. The main findings of this study are summarized in section 8 with a note about future work.

TABLE 1. Four versions of the FSU global coupled climate models and their nomenclature used in this paper.

Model	Radiation scheme	Convection scheme
ANR	New, based on band model	Arakawa–Schubert (Grell 1993)
AOR	Old, based on emissivity–absorptivity	Arakawa–Schubert (Grell 1993)
KNR	New, based on band model	Modified Kuo (Krishnamurti et al. 1980)
KOR	Old, based on emissivity–absorptivity	Modified Kuo (Krishnamurti et al. 1980)

2. Models and datasets

Four versions of the coupled Florida State University (FSU) General Spectral Model (GSM) were used in our study. These models vary from each other in the parameterization of radiation and convection. Two radiation schemes, one based on band model (referred as new in this paper) and the other based on emissivity–absorptivity (Krishnamurti et al. 2002, referred to as old in this paper) were used in combination with two different convection schemes (viz., the Arakawa–Schubert and the Kuo). The Arakawa–Schubert scheme is a simplified version of the original scheme (Arakawa and Schubert 1974) by Grell (1993). The Kuo convection scheme used in our study was based on Krishnamurti et al. (1980) and Krishnamurti and Bedi (1988), which is a modified version of the parameterization introduced by Anthes (1977). Table 1 lists these features of the four models and their nomenclature used in this paper. Details of the FSU coupled model are given in Larow and Krishnamurti (1998).

The atmospheric component of the model has a spectral triangular truncation at wavenumber 63 (T63), which corresponds to a horizontal grid spacing of roughly 1.875°. It has 14 vertical sigma levels with more closely spaced levels near the surface and tropopause. The ocean model is a version of the Hamburg Ocean Primitive Equation global (HOPE-G) model (Wolff et al. 1997), which uses the Arakawa E grid. The horizontal resolution of the ocean model is 5° in longitude and 0.5°–5.0° in latitude with higher resolution near the equator. The ocean was first spun up for 11 yr with observed wind and SST. Next, a coupled assimilation procedure was used to create oceanic initial conditions for the coupled forecast by the FSU–GSM. Details of this assimilation procedure is provided in section 5.

The primary observational dataset that is used in this study was prepared by the National Climate Centre of the IMD, Pune, India. As many as 2140 rain gauge–based precipitation observations over India were used to obtain a $1.0° \times 1.0°$ gridded datasets (Rajeevan et al. 2006). The

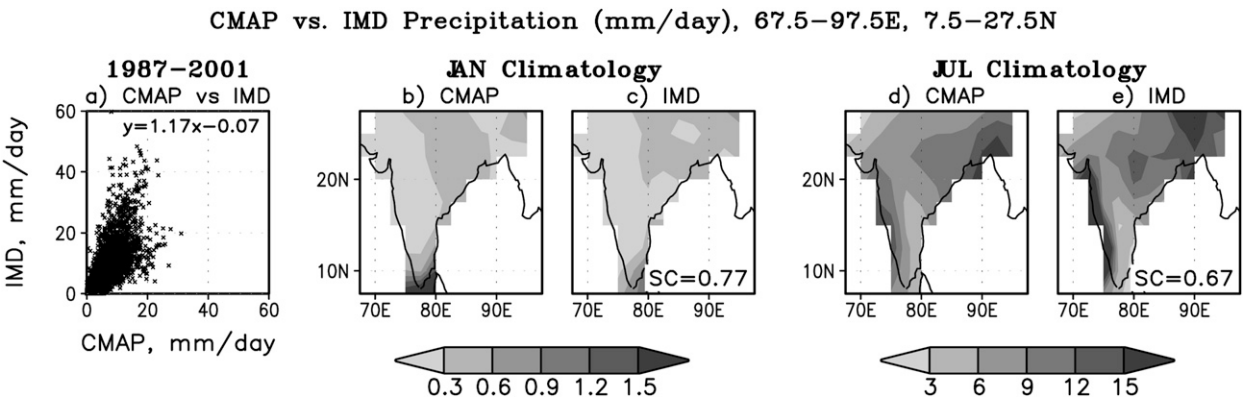

FIG. 1. (a) Grid-by-grid relationship between CMAP and IMD precipitation over 7.5°–27.5°N, 67.5°–97.5°E during all the months of 1987–2001. The linear relationship between these two datasets is indicated. (b),(c),(d) January and July climatology of CMAP and IMD precipitation during 1987–2001. The spatial correlation between these two datasets is indicated for IMD.

spatial interpolation procedure from the irregularly spaced rain gauge network to equal angle grid was adapted from Shepard (1968). The temporal resolution of this precipitation dataset is 1 day, and available from 1950 to 2004. This is a long and comprehensive dataset available for studies of monsoons over the Indian region at different time scales (Rajeevan et al. 2006). In this study, we have created a monthly mean dataset for the period 1987–2001 from this daily IMD observations. This period was constrained by the availability of the coupled model datasets. However, there were 6 yr during this 15-yr period when the Indian region experienced seasonal precipitation far from the normal. And the years 1987, 1988, 1994, and 2000 were extreme among those 6 yr. We have shown, in this manuscript, the forecast skill during all individual extreme years.

The coarse-resolution (2.5° × 2.5°) monthly mean precipitation was obtained from the Climate Prediction Center (CPC) Merged Analysis of Precipitation (CMAP; Xie and Arkin 1997). Forecasts from member models were averaged to the CMAP grid to calculate their skills before downscaling. Figure 1 shows the comparison between these two observational datasets used in our study. In Fig. 1a, the grid-by-grid relationship between CMAP and IMD precipitation over the Indian region (7.5°–27.5°N, 67.5°–97.5°E) is shown for all the months during 1987–2001. Since CMAP and IMD grids are different in resolution, the IMD grid (higher resolution) was regrided to the CMAP grid (lower resolution) using a box averaging procedure (averages over all the fractional grids of IMD those fall within a CMAP grid). It is to be noted that IMD precipitation is slightly higher compared to CMAP precipitation over most of the precipitation ranges. This could be due to differences in observational sources as well as the resolution between these two datasets. CMAP uses satellite, radar, and rain gauge observations to construct their monthly mean precipitation product (Xie and Arkin 1997). However, IMD-based precipitation is only based on dense rain gauge observations (Rajeevan et al. 2006). The linear relationship between these two datasets is indicated inside Fig. 1a, which shows that there is almost no constant bias between precipitation obtained from CMAP and IMD (intercept = 0.07 mm day^{-1}). On the other hand, the CMAP precipitation has to be scaled by a factor of 1.17 to match the IMD rainfall on the same grid.

Figures 1b–e show the climatology of January and July precipitation over the Indian region from CMAP and IMD observations. The spatial correlation between these two datasets is indicated inside the respective panels. During January, CMAP shows higher precipitation at the southernmost tip of the Indian peninsula compared to the IMD datasets. On the other hand, during July, the IMD datasets show higher precipitation over the west coast of India and over the northeast Indian region compared to the CMAP. However, the overall spatial pattern between these two datasets is similar during both the months (spatial correlations of 0.77 and 0.67, respectively, during January and July). Therefore, it can be concluded that these two datasets are close enough to compare skill scores between coarse resolution and downscaled model forecasts.

3. The downscaling strategy

Our downscaling strategy is as follows. We started with monthly mean datasets at 2.5° × 2.5° resolution from four FSU models, and monthly mean datasets at 1.0° × 1.0° resolution from IMD observations. The common time period of these datasets is 1987–2001. Now, the coarse-resolution model precipitation over the Indian monsoon region was bilinearly interpolated to

the higher-resolution grid of the observed IMD precipitation:

$$M' = \text{Interp}(M), \tag{1}$$

where Interp() is the bilinear interpolation operator and M is the model forecast field. This provided $1.0° \times 1.0°$ resolution interpolated datasets from the four models during each month of 1987–2001 (15 yr). Next, all the 12 months of the first year of model forecasts were kept aside and the rest of the 14 yr of data, once for each month and each grid, were used to calculate coefficients of the following equation:

$$O = aM' + b + \epsilon, \tag{2}$$

where O and M' are the observed and interpolated model forecast of rainfall on that grid, respectively; a and b are regression coefficients (the slope and intercept of the linear fit, respectively); and ϵ is the error term. The regression procedure is a least squares linear fit that minimizes the absolute value of the error term ($|\epsilon|$). Once these regression coefficients (a and b) are obtained, they are used in the forecast year to calculate downscaled model precipitation:

$$M'' = aM' + b, \tag{3}$$

where M'' is the downscaled forecast of the model [other symbols are same as in Eq. (2)]. Note that, in the above equation, the values of a and b are obtained from the least squares linear regression described by Eq. (2). Hence, one set of coefficients are calculated for every grid point and for every month of the year. The entire procedure is repeated for every year of the 15 yr of datasets (cross validation; Déqué 1997). This spatial and seasonal dependency in regression coefficients is necessary to take into account the regional and seasonal variation of the model skills in predicting monthly precipitation over India. This downscaling strategy, when applied to every grid in the domain of interest, corrects model bias over numerous regions such as orography, vegetation, land–sea boundary, etc. This is mainly possible because the observed precipitation datasets is rain gauge based and is free from any error arising from those factors.

4. Superensemble methodology

The superensemble methodology (Krishnamurti et al. 1999, 2000b) combines multiple model forecasts based on their past performance to make a consensus forecast. To obtain the past performance, the forecast time series is divided into a training period and a forecast period. The model forecasts are regressed in the training period with the observed counterpart to obtain weights:

$$G = \sum_{t=1}^{N_{\text{train}}} (S'_t - O'_t)^2, \tag{4}$$

where G is the error term that is minimized to obtain the weights, N_{train} is the length of the training dataset, and S'_t and O'_t are the superensemble and observed field anomalies, respectively, at training time t. The outcome of this regression is statistical weights a_i ($i = 1, 2, \ldots, N$; N being the number of models) assigned to every model in the suite. These weights are then passed on to the forecast phase to construct superensemble forecast:

$$S = \overline{O} + \sum_{i=1}^{N} a_i(F_i - \overline{F}_i), \tag{5}$$

where $\overline{O}$ is the climatology of the observed field, and F_i and $\overline{F}_i$ are the forecasts and forecast climatology, respectively, for the ith model. The summation is taken over the N-member models in the suite. The observed and model climatology fields are the mean over the training period during every calendar month. The coefficients are estimated my minimizing the error term of Eq. (4). This method is illustrated in Fig. 2a. The superensemble differs from the conventional bias-removed forecasts in the assignment of weights to the member models. In the bias-removed forecast, an equal weight of $1/N$ is assigned to every model where N is the total number of models. For the superensemble, model weights are based on their performance in the training phase, and can even attain a negative value if the model anomalies are negatively correlated with that of the observation in the training phase (Chakraborty et al. 2007). Moreover, for the superensemble, the weights vary geographically, which takes into account the regional variation of skills of the member models. This varied weights leads to a better forecast by the superensemble compared to the bias-removed ensemble mean forecasts (Stefanova and Krishnamurti 2002; Chakraborty and Krishnamurti 2006).

The seasonal climate forecasts of the superensemble uses a variation of the above, which was shown to have performed better than the conventional superensemble methodology (Yun et al. 2005). In this variation, synthetic forecasts for each of the member models are created from their original forecast time series using linear regression with their observed counterpart in the EOF space. This methodology is as follows.

The observed time series are expanded in terms of principal component (PC; in time) and empirical orthogonal function (EOF; in space):

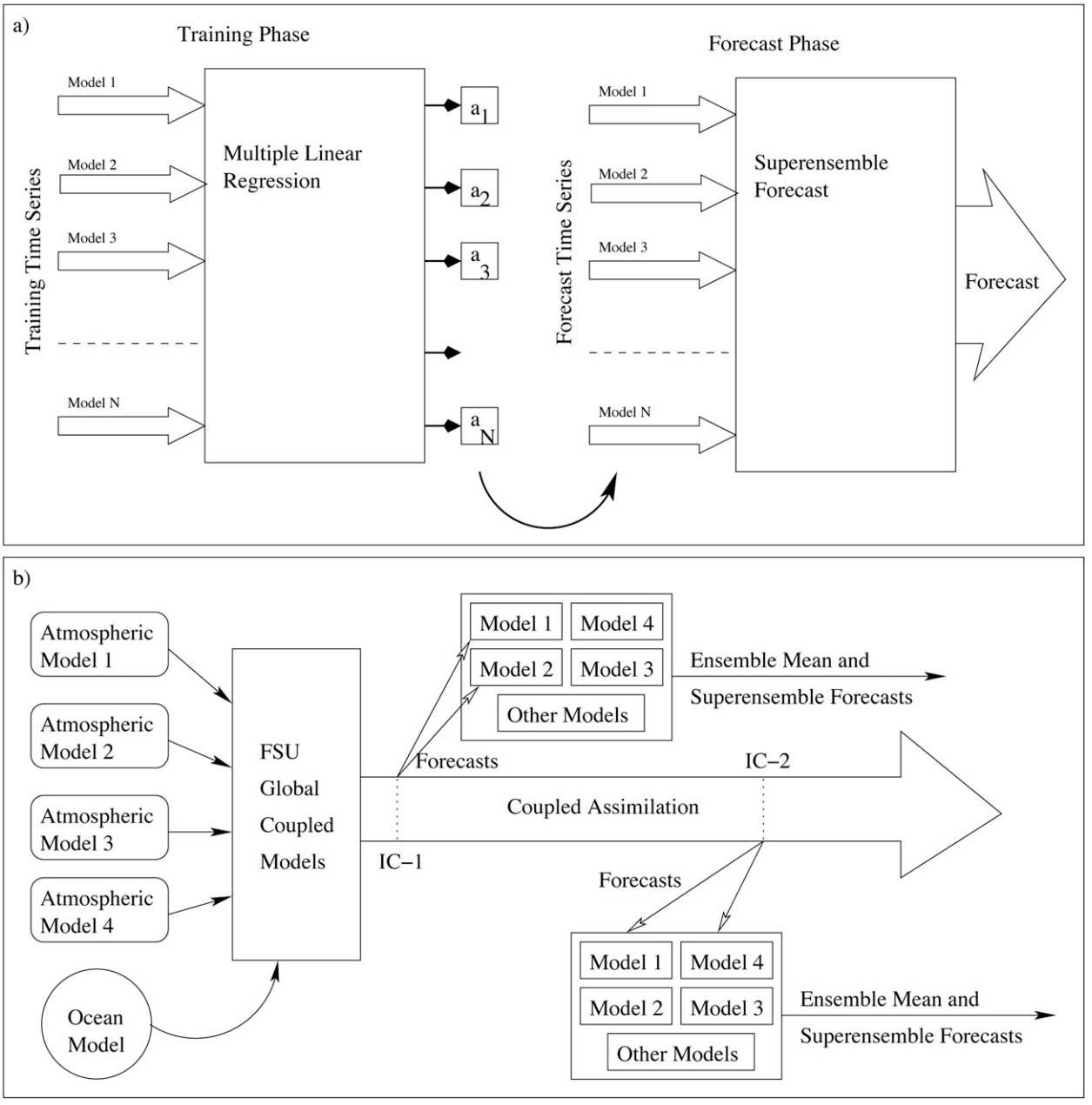

FIG. 2. (a) Superensemble methodology and (b) the coupled assimilation procedure for the FSU global atmosphere–ocean coupled models.

$$O(x,\ t) = \sum_{k=1}^{M} P_k(t)\ .\ \Phi_k(x), \tag{6}$$

where P_k denotes the PC time series; Φ_k is the EOF component of the kth mode, which is a function of space alone; and M is the number of modes selected. The number of modes corresponding to 99% of the variance in the original data are retained in our expansions. This corresponds to about 85 PC components both in the model forecasts and in the observed datasets. It was noted that the forecast is not sensitive to the number of modes as long as it explains more than 95% of the total variance. Choice of the number of modes those correspond to less the 95% of the total variance in the dataset introduced a large error in the synthetic superensemble forecast. The skill of the synthetic superensemble thus created did not exceed that of the conversional superensemble.

Similar to the observed, the model datasets are also expanded:

$$F_i(x,\ t) = \sum_{k=1}^{M} F_{i,k}(t)\,\phi_{i,k}(x), \tag{7}$$

where i denotes the ith model in the suite, $F_{i,k}$ is the PC time series for the kth mode of the ith model, and $\phi_{i,k}$ is the EOF.

Now, every mode of the PC time series of the models are regressed against the corresponding observed counterpart to obtain weights for each model. In this procedure, the kth mode of the PC time series of the observation is written as a linear combination of that of the member models:

$$P_k(t) = \sum_{i=1}^{N} \alpha_{i,k} F_{i,k}(t) + \epsilon_{i,k}, \tag{8}$$

where i is the ith member in the ensemble, $\alpha_{i,k}$ is the weight to the ith model for mode k, and $\epsilon_{i,k}$ is the error term. The weights ($\alpha_{i,k}$) are estimated using multiple linear regression that minimizes the variance of the error $E(\epsilon_{i,k}^2)$. The regression-obtained PC time series thus obtained can be written as

$$F_{i,k}^{\text{reg}}(t) = \alpha_{i,k} F_{i,k}(t).$$

These, when combined with the spatial EOF, provides the synthetic forecast dataset:

$$F_i^{\text{reg}}(x, t) = \sum_{k=1}^{M} F_{i,k}^{\text{reg}}(t)\Phi_k(x), \tag{9}$$

where $\Phi_k(x)$ denotes the EOF components of the observation. The above exercise is repeated for every model in the ensemble. To forecast a particular year, we have used the entire model forecast time series. However, the observational data for that year was substituted by the ensemble mean of the member models. This was required to remove any dependency of the results with available observation during the forecast year. The synthetic dataset thus obtained is sent to the original superensemble algorithm for final superensemble forecast. Further details of this methodology are provided in Yun et al. (2005), Krishnamurti et al. (2006b), and Chakraborty and Krishnamurti (2006). It has been shown in these studies that for seasonal climate forecasts the synthetic superensemble methodology performs better than the conventional superensemble methodology. In this paper we will use the term superensemble to refer to synthetic superensemble.

5. Coupled assimilation

Prior to the start of each seasonal forecast we include a coupled assimilation. This procedure, based on Krishnamurti et al. (2000a) is outlined in Fig. 2b. This includes the following steps.

a. Oceanic spinup

The ocean state undergoes a spinup where 11 yr (1976–86) of monthly mean observed surface winds [obtained from the 40-yr European Centre for Medium-Range Weather Forecasts (ECMWF) Re-Analysis (ERA-40)] and monthly mean SSTs (based on Reynolds and Smith 1994 datasets) were used. This component of ocean data assimilation is carried out using a continuous Newtonian relaxation technique (Krishnamurti et al. 2000a). This spinup generates ocean currents, oceanic temperature, and distributes the salinity fields in three dimensions that acquire an equilibrium, with respect to the prescribed surface wind stress and the SSTs. This feature of the modeling does not assure an equilibration for the deeper oceans that may require much longer time scales (compared to 11 yr). Because the upper oceans are considered more important for seasonal forecasts (of monsoon), this may not be a major limitation.

b. Coupled assimilation

Daily coupled assimilation follows the 11-yr spin-up phase. This is a continuous assimilation that covers the period 1987–2001. The atmospheric part of the coupled assimilation follows our previous study Krishnamurti et al. (1991). Here we include a physical initialization of observed rainfall based on Tropical Rainfall Measuring Mission (TRMM) data files from Kummerow et al. (1998). The ECMWF datasets provides all of the gridded initial variables such as the wind components u, v, and $\dot{\sigma}$, and the temperature, humidity, and surface pressure distributions. The atmospheric spinup is done using a Newtonian relaxation of these base variables constrained to the physical initialization of the improved rain rates. The Newtonian relaxation calls for hard and soft nudging for different variables to enable the model to essentially retain the rotational part of the wind from the ECMWF data analysis at the end of our assimilation. However, it permits the other fields such as humidity, surface pressure, vertical motions, and diabatic heating to adjust to the imposed rains. This coupled assimilation is shared by all of the member models of our suite.

6. Seasonal forecast experiments

Seasonal forecasts with the four FSU coupled models are performed for the years 1987–2001. Two forecasts

per month, one starting at the middle and the other starting at the end of each month were carried out for each of the four member models. This study uses the model outputs that started only at the end of a month during our study period. The oceanic initial condition was taken from the output of the coupled assimilation phase. The atmospheric initial condition was obtained from ECMWF 0.5° × 0.5° analysis datasets. The length of each forecast was 90 days. Forecast fields averaged from days 1 through 30 is termed as month 1 in this study. Months 2 and 3 of forecasts follow similarly. The string of all month-1 forecasts from January 1987 to December 2001 (180 time points) constitute the month-1 forecast time series in our study. Similarly, month-2 forecast time series start on February 1987 and end on January 2002, and month-3 forecasts start on March 1987 and end on February 2002.

In this paper we will illustrate forecast skills of the models, their ensemble mean, and the superensemble before and after downscaling. All model forecasts before downscaling were interpolated to a common 2.5° × 2.5° grid to compare with the CMAP datasets. The ensemble mean and the superensemble forecasts were created from these 2.5° horizontal resolution, monthly forecast time series. These forecast products are referred as coarse resolution or CRes in this paper.

To construct downscaled forecasts, the monthly mean datasets from every model were first downscaled using the proposed algorithm to the 1.0° horizontal resolution grid. Next, this downscaled forecast time series from the models were used to calculate downscaled ensemble mean and superensemble forecasts. The downscaled forecasts are termed DScl in this paper.

7. Results

a. Skills of uninterpolated and interpolated rainfall

Prior to the statistical downscaling we bilinearly interpolated the model forecast rains from a 2.5° × 2.5° longitude–latitude grid to a 1.0° × 1.0° longitude–latitude grid. These two products, the uninterpolated and the interpolated rains, were compared with the CMAP- and IMD-based precipitation estimates, respectively. The 15 yr (1987–2001) climatology of coarse resolution (2.5°) and interpolated (1.0°) forecasts of precipitation for month 2 during July and December from the four member models are illustrated in Figs. 3a–t. The RMS errors (in mm day^{-1}) of the precipitation climatology for this month along with months 1 and 3 of forecasts are shown in Figs. 3u–z. The RMS errors were calculated using the following equation:

$$\text{RMS error} = \sqrt{\frac{1}{N}\sum_{i=1}^{N}(F_i - O_i)^2}, \qquad (10)$$

where F_i and O_i are forecast and observed fields, respectively, at the ith grid point. Here N is the total number of grid points in the domain. There are some obvious model to model differences in these 15-yr averages. The uninterpolated model precipitation has RMS errors in the range of 1.4–6.4 (1.9–6.1 for month 2) mm day^{-1} (when verified against the CMAP rains). The interpolated rains are essentially the same fields as the uninterpolated ones and these have RMS errors of the order of 1.5–13.6 (1.9–13.4 for month 2) mm day^{-1} for months 1, 2, and 3 of forecasts. The IMD rains were used here as the benchmark for this higher resolution. These large errors arise because the IMD rain gauges measure extreme local rains (e.g., high along the west coast and low in the rain shadow region of south-central India). Those levels of high or low local rains are not predicted by large-scale models. When this large-scale-averaged precipitation by the coarse-resolution models is interpolated to finer grids, it leads to higher RMS errors because the spatial variability of high-resolution precipitation within the large-scale grid is not captured by the interpolation procedure. The reason why we are presenting these is to show in a later section of the paper that this same product that carries these large local errors can be very much improved by deploying a statistical downscaling and a multimodel superensemble based on these downscaled member models.

b. Spatial distribution of downscaling coefficients

The coefficients a and b of the linear regression [Eq. (2)] that relates interpolated model-predicted rainfall against the high-resolution observed IMD counterpart provide useful information for the systematic errors of each model. A slope of 1.0 would imply that the large-scale model has rain equal to the high-resolution rain of IMD at all rainfall rates after removing the constant bias (the intercept b). The slope of 1.0 also conveys that the rate of change of model rain is consistent with that of the observed. A faster (slower) rate of change of rain by the model implies a slope $0 < a < 1$ ($a > 1$). A negative value of a indicates that model rain is lower (higher) then observation in the high (low) observed precipitation range. On the other hand, b implies the constant bias of the model compared to the observation at any precipitation range. A positive (negative) value of b indicates that the model rain was lower (higher) compared to the observation.

The spatial distribution of the slope and intercept (a and b) during July and December for month 2 of

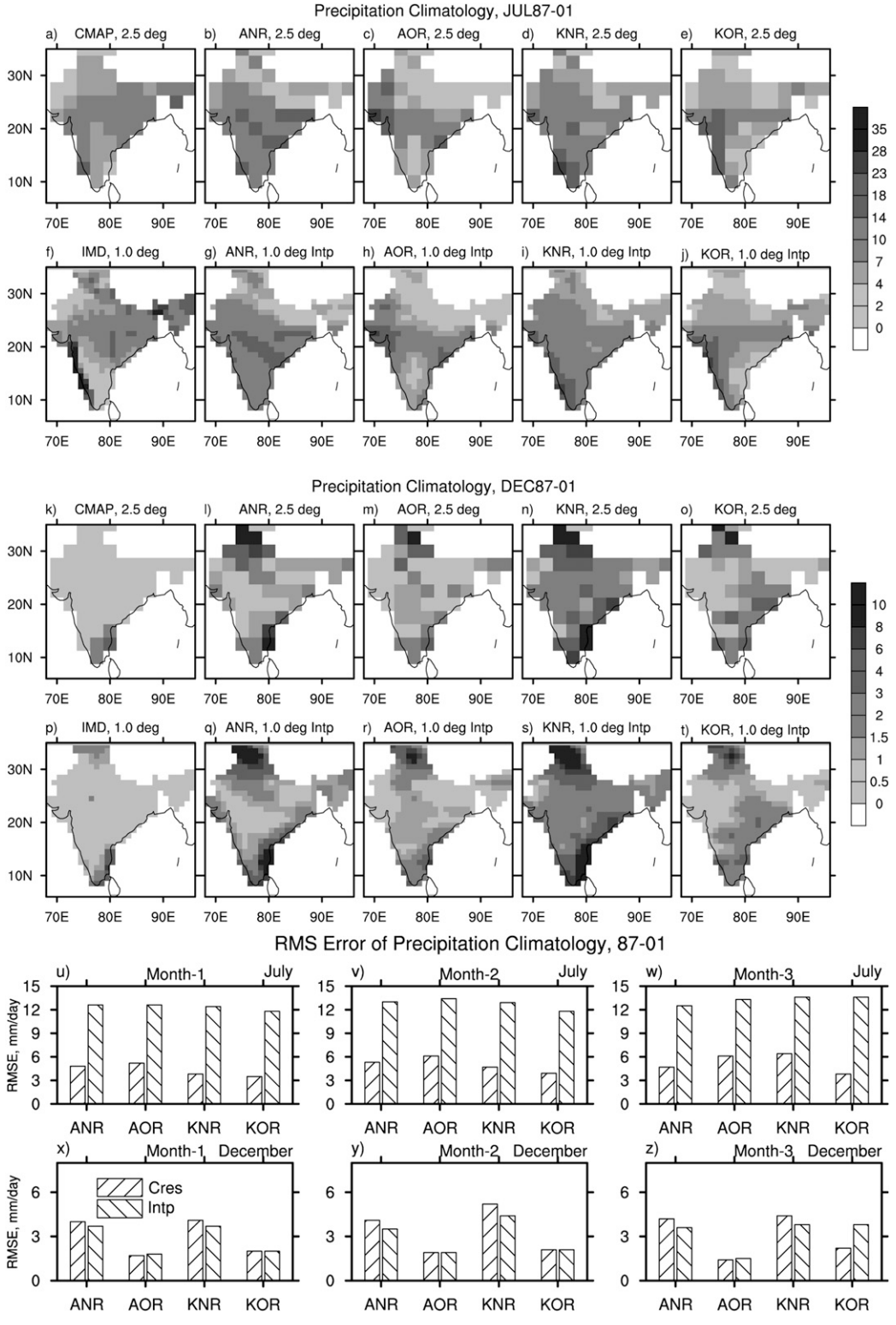

FIG. 3. Observed and forecast climatology of coarse-resolution and interpolated precipitation (mm day^{-1}) during (a)–(j) July and (k)–(t) December 1987–2001 for month 2 of forecasts. (u)–(z) The RMS error (mm day^{-1}) of the coarse-resolution (Cres) and interpolated (Intp) forecast fields when compared with the corresponding resolution observed datasets.

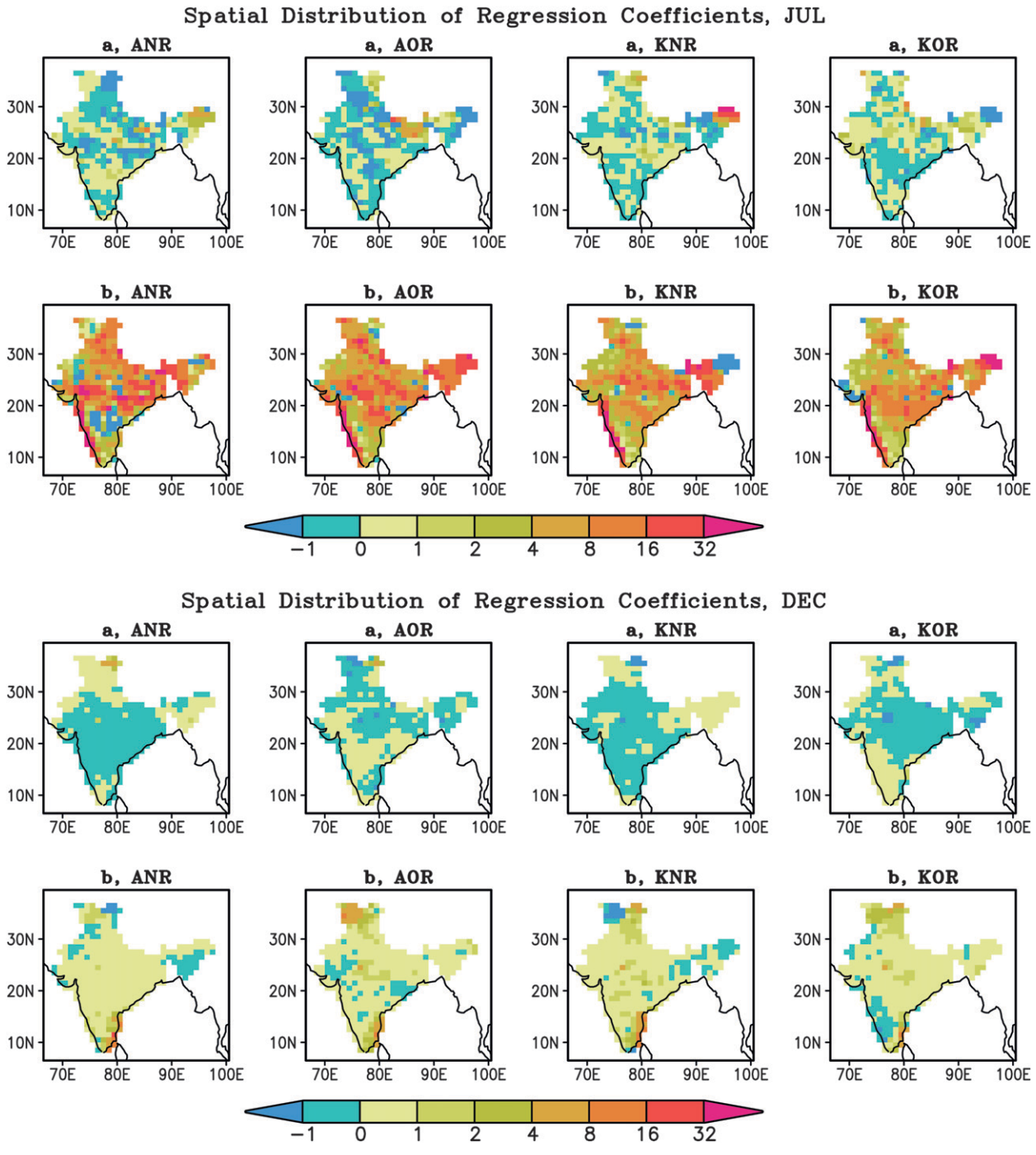

FIG. 4. Downscaling coefficients a (slope) and b (intercept) during July (first and second rows) and December (third and fourth rows) 1987–2001 for month 2 of forecasts.

forecasts for the four member models are presented in Fig. 4. The distribution of the coefficients are quite different during summer and winter seasons because of the nature of the rainfall. The large convective rain of the summer season is systematically underestimated by all of the models over most of this domain. Those underestimates are strongly reflected in the intercept b, which carries values as high as 16–32 mm day^{-1}. The large-scale model rain interpolated to a fine mesh need such large corrections locally to arrive at the level of the heavy observed convective rains. There is a systematic overestimation of rains at all ranges ($0 < a < 1$)

over south-central India by the model that utilized the Arakawa–Schubert cumulus parameterization scheme for its convection and a band model for its radiative transfer (ANR). This feature is less pronounced in the other models. There are many smaller-scale features in the slope alternating between ±1. This arises because of the smoother larger scales of model rains and heavier mesoscale features of the observed rains. In the steep orographic regions of the Himalayas, some models carry large errors of the order of 16–32 units for the slope parameter, these are indicative of underestimates of heavy orographic rains by the large-scale models where the observed rains have been much larger intensity.

The four models carry somewhat different fields of the slope *a* during December (Fig. 4, third and fourth rows). The ANR model carries a positive slope (0 to +1) over north of 30°N and a negative slope (0 to −1) south of 30°N. This, along with the fact the value of intercept *b* is small positive south of 30°N latitude, implies that this model overestimates low rains and underestimates heavier rains over this region. North of 30°N, in the winter season, most of the rains occur from western disturbances. That is similar to precold frontal rains and is largely stratiform in nature. The combination of Arakawa–Schubert cumulus parameterization and the band model for the radiative transfer (ANR) appears to underestimate stratiform rains. The other models seem to carry less bias in this region. Such inferences, however, need to be taken with a word of caution. It was noted in Krishnamurti and Sanjay (2003) that a physical parameterization scheme within two different models can show different behavior even if all other physics and initial datasets were kept identical. A physical parameterization scheme's behavior also depends strongly on the rest of the model within which it resides. Large-scale global model and regional model can differ in resolution, advective algorithm, and boundary conditions and can thus affect the behavior of a cumulus parameterization quite differently. Most models carry values for the intercept *b* between 0 and 1 over most of India, implying that this systematic error (underestimate) for rainfall is of the order of 0–1 mm day^{-1}. However, all models underestimate rainfall by 2–8 mm day^{-1} near the southeastern coast of India where winter monsoon dominates over summer monsoon. Similar underestimation of precipitation is noticed over the mountainous regions north of 30°N.

The coefficients shown in Fig. 4 are not sensitive to the number of years (data points) chosen for the regression. Figure 5 shows how the values of *a* and *b* changes with the number of years used in the least squares linear regression procedure at a location near the southwest coast of India (13.5°N, 75.5°E). At first, 3 yr of data were taken and coefficients were calculated. Addition of more years to the regression database changes the values of the coefficients wildly at first. However, when the number of years crosses 10, both the values stabilize and does not show large sensitivity to the number of data points. This is true during both winter (December) and summer (July), except for coefficient *b* during July. During this month, the value of *b* was not as stable as was seen during December. However, the variation during July after the number of months cross 7 was much less as compared to that when less than 7 months were considered to calculated the regression coefficients. The above result shows that our choice of 14 yr of training to calculate the downscaling coefficients for the forecast year is adequate for this study.

c. Downscaled climatology

Each of the model forecasts for months 1, 2, and 3 were downscaled using the observed IMD high-resolution rains for the respective months. Figure 6 shows the June–September climatology of coarse- and high-resolution (downscaled) precipitation from CMAP- and IMD-based observations along with the forecasts from member models, their ensemble mean, and the superensemble before and after downscaling for months 1, 2, and 3 of forecasts. Within each forecast panel, we have shown the RMS error of the climatology fields when compared with the respective resolution observation. We note that both the observed (CMAP) and the coarse-resolution models fail to show the strong west coastal heavy rains in their climatology; furthermore, the southern India rains (south of 15°N) were absent in these climatologies. The RMS errors for the climatology of large-scale models carry values from 2.47 to 5.54 mm day^{-1}. The superensemble based on these large-scale models is able to reduce these errors. The climatology of the downscaled models, when compared with the high-resolution IMD-based precipitation observation, show much higher skills compared to their coarse-resolution counterpart. It was possible to obtain the RMS error of monthly climatology of the member models of the order of 0.01–0.10 mm day^{-1}. This is one of the promising aspects of the proposed downscaling. Both the ensemble means and the large-scale downscaled models provide the climatology of precipitation that shows much higher skills compared to the corresponding coarse-resolution counterpart. The RMS error of the climatology field from the superensemble was of the same order as that of the large-scale models and their ensemble mean.

d. Forecast skills over a seasonal time scale

In this section the skills of forecasts over seasonal time scales are measured using RMS error and equitable

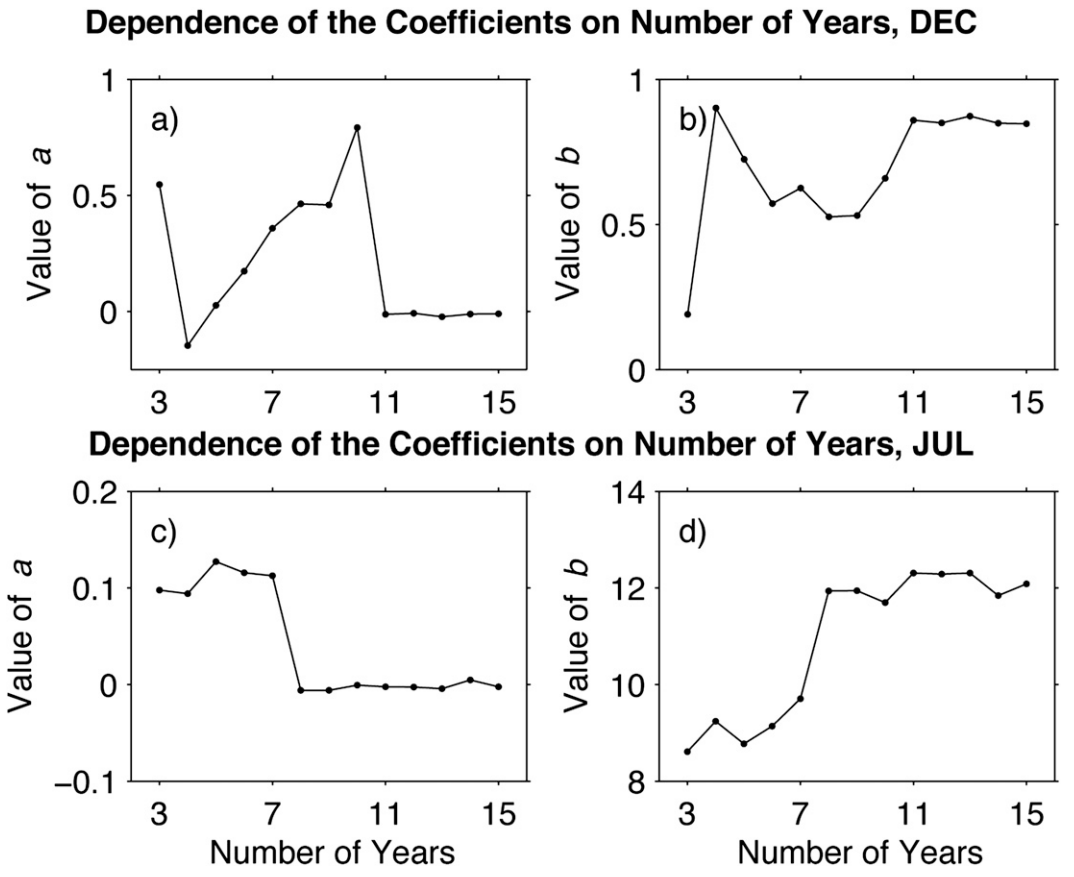

FIG. 5. Dependence of the downscaling coefficients a (slope) and b (intercept) on the number of years in the training period during (a),(b) December and (c),(d) July for month 3 of forecasts at 13.5°N, 75.5°E (near the southwest coast of India). The values of the regression coefficients get stabilized when more than about 10 yr of data are used in the training period.

threat score (ETS). The ETS is defined as (Rogers et al. 1996):

$$\text{ETS} = \frac{H - E}{F + A - H - E}, \tag{11}$$

where F and A are the number of grids where forecast and observed fields exceed a specified threshold, respectively; and H is the number of grids that correctly forecast more than the specified threshold (also termed as ''hit''). In other words, H is the number of grids where both the observed and forecasted field cross the threshold; and $E = F \times A/T$, T being the total number of grids over the region. ETS values can range from $-\frac{1}{3}$ to 1. The higher the ETS, the better the forecast. An ETS value of 1 indicates perfect forecast skill.

The ETS for months 1, 2, and 3 of forecasts for the southwest Indian domain during June–September of 1987–2001 are shown in Fig. 7. ETS from both coarse-resolution and downscaled forecasts are shown to illustrate the marked improvements obtained from the downscaling methodology. The threat scores of the rains were less than 0.1 for the large-scale models for all the months 1, 2, and 3 of the forecasts. The downscaled versions of these models show ETS values as high as 0.4–0.6. The member models and the superensemble perform the best (ETS values reach peak) for precipitation thresholds of 15 and 20 mm day^{-1}. The threat scores for rains in excess of 35 mm day^{-1} are as high as 0.4, which is not well predicted by the large-scale models. Similar improvements are obtained for the ensemble mean forecasts as well. It is interesting to note that the ETS score for the superensemble based on forecasts of the large-scale models follow closely to that of the downscaled superensemble for rain rates $\leq$10 mm day^{-1}. This shows that the superensemble based on large-scale models is able to predict low rains ($<$15 mm day^{-1}) as well as the downscaled higher-resolution superensemble. However, at higher rain rates ($>$15 mm day^{-1}) the skill of the superensemble falls sharply. Figure 7 conveys the

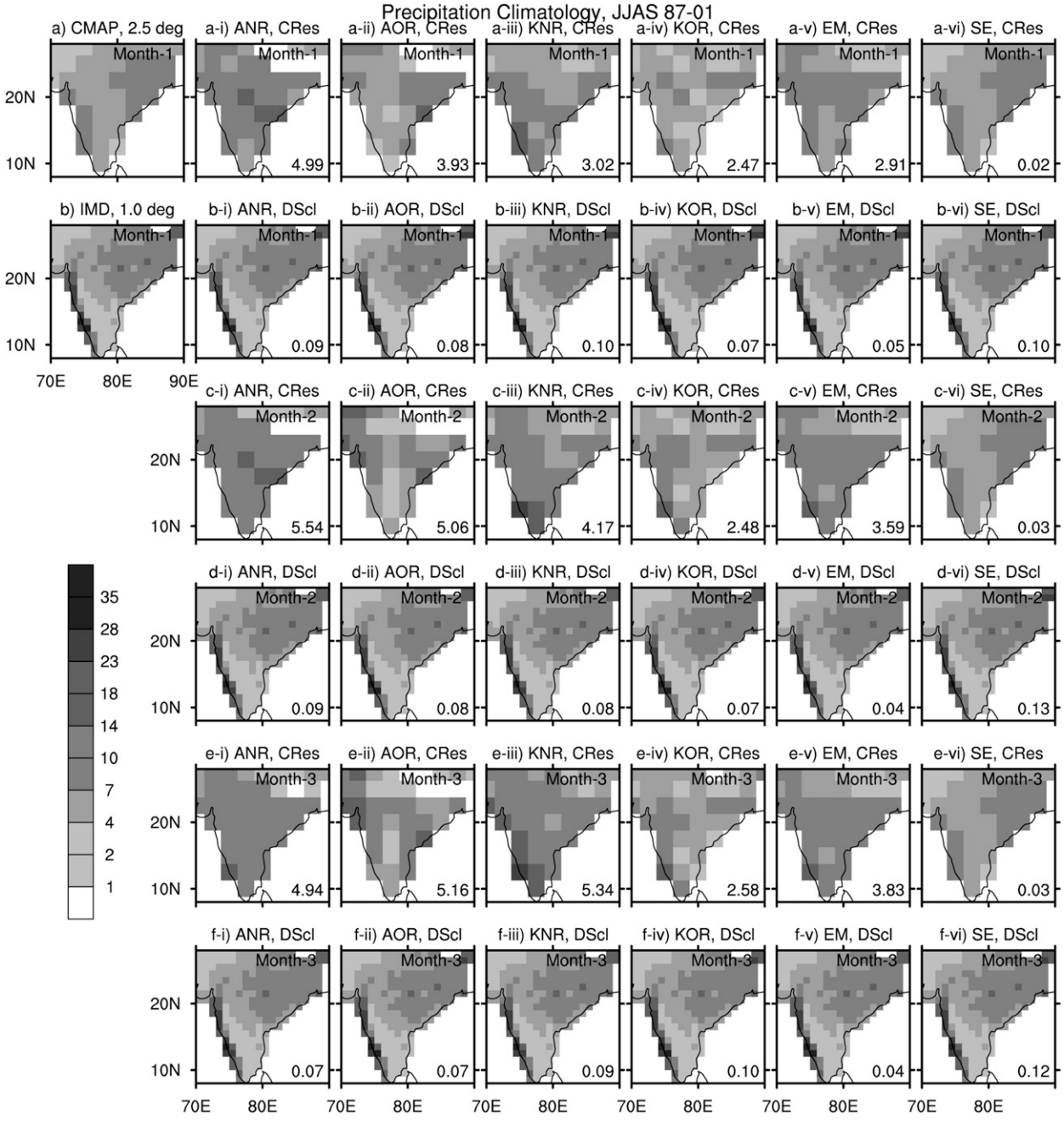

FIG. 6. Precipitation climatology (mm day^{-1}) from observations, four member models, their ensemble mean, and the superensemble during June–September of 1987–2001 in coarse resolution (CRes) and after downscaling (DScl) for months 1, 2, and 3 of forecasts. The RMS errors of the forecast fields are indicated.

most important results of the present study that show the effectiveness of the combination of statistical downscaling and the multimodel superensemble.

Table 2 shows the RMS error of downscaled precipitation forecasts from the four member models, the observed climatology, their ensemble mean, and the superensemble during July 1987–2001 over the Indian monsoon region (8°–28°N, 70°–90°E). To calculate the superensemble forecast, the observed climatology was considered as a member model in this case. The last column indicates the confidence level by which the RMS error of the superensemble differs from the mean RMS error of the member models. The confidence level was calculated using a Student's *t* test (Chakraborty and

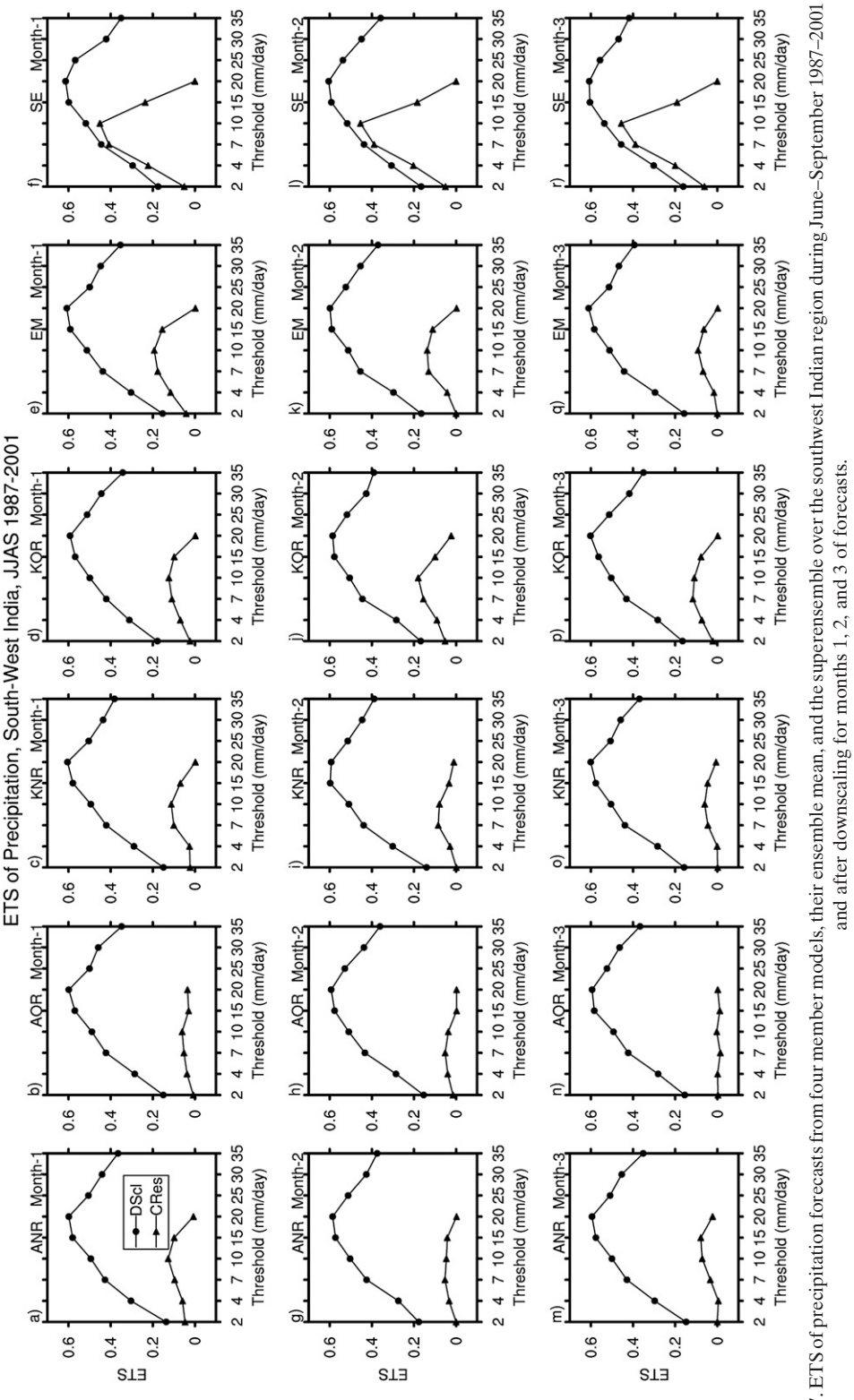

FIG. 7. ETS of precipitation forecasts from four member models, their ensemble mean, and the superensemble over the southwest Indian region during June–September 1987–2001 before and after downscaling for months 1, 2, and 3 of forecasts.

TABLE 2. RMSE of month-3 precipitation forecasts from the four FSUGSMs (ANR, AOR, KNR, KOR), observed climatology (CLM), the ensemble mean (EM), and the superensemble (SE) during July 1987–2001 over 8°–28°N, 70°–90°E. The confidence level by which the superensemble forecast differs from the ensemble mean forecast is indicated in the last column (clev).

Yr	ANR	AOR	KNR	KOR	CLM	EM	SE	clev
1987	6.31	6.78	5.99	6.71	6.11	6.23	5.91	93.8
1988	7.11	6.87	6.74	6.81	6.84	6.80	6.57	97.0
1989	5.61	6.07	5.58	5.65	5.70	5.57	5.55	77.9
1990	5.75	5.64	5.91	5.39	5.32	5.39	5.36	93.5
1991	5.33	5.78	5.26	5.34	5.25	5.24	5.08	93.9
1992	5.52	4.64	4.24	4.73	4.38	4.56	4.28	84.3
1993	5.59	5.98	5.74	5.60	5.35	5.47	5.07	99.4
1994	6.93	6.90	6.71	6.73	6.71	6.70	6.47	99.1
1995	5.81	5.44	6.02	6.34	5.52	5.67	5.20	96.6
1996	4.32	4.51	4.62	4.89	4.28	4.38	4.19	95.4
1997	4.96	6.12	6.03	5.69	5.76	5.48	5.61	24.5
1998	4.48	4.76	5.96	5.03	4.33	4.58	4.37	87.8
1999	5.32	4.70	4.65	4.46	4.53	4.57	4.32	91.1
2000	4.48	5.11	5.12	4.99	4.76	4.71	4.29	97.5
2001	6.06	5.80	6.10	5.79	5.86	5.80	5.71	92.9
Mean	5.57	5.67	5.64	5.61	5.38	5.41	5.20	99.9

Krishnamurti 2006). Note that during most of the years (and on the average, indicated by mean) the RMS error from the superensemble was less compared to those of the member models, the climatology, and their ensemble mean. The confidence level exceeds 95% (90%) during 6 (11) yr out of the 15-yr simulation. Note also that during 1987 and 1988, which were characterized by lower- and heavier-than-normal summer monsoon rainfall over the Indian region, respectively, the skill of the superensemble was higher than the member models and the ensemble mean. The mean RMS error of the 15 yr show a robust improvement (confidence level is 99.9%) in forecast skills of the downscaled superensemble compared to the downscaled member models and the ensemble mean. When compared with the RMS error of the climatology, we find that on an average the superensemble performs better than the benchmark observed climatology. On the other hand, the ensemble mean does not show higher skill when compared to this benchmark. These results show that the combination of downscaling and superensemble can provide a high skill for monsoon rainfall forecasts over the Indian region.

e. Forecast skills during extreme monsoon years

Summer monsoon precipitation over the Indian region encountered two consecutive extreme years of opposite anomaly during our 15 yr of study period. During 1987, the July (June–September) mean precipitation over the region 8°–28°N, 70°–90°E (land area and where IMD observations are available) was 32% (19%) below the 15-yr climatology in the CMAP-based observation. Corresponding decrease in the IMD-based data was 25% (18%). On the other hand, during 1988, the July (June–September) mean precipitation over the same region was 16% (11%) above normal in the CMAP datasets and 21% (12%) above normal in the IMD datasets. The spatial pattern of the anomaly of precipitation during June–September 1987 and 1988 from IMD-based observations are shown in Figs. 8a,d, respectively. Note that, although domain-averaged precipitation over this region was below normal during 1987, this decrease was mainly over north, central, and south India. Over northeastern India there was a strong positive anomaly of precipitation in this year. On the contrary, during 1988 (Fig. 8d), the northeastern Indian region suffered below-normal precipitation when rest of the Indian region (mainly south-central India) experienced higher-than-normal precipitation. In this section we illustrate how the member models and the superensemble predicted this seesaw in the dipole structure of precipitation anomaly during 1987 and 1988.

Figures 8b,c show the precipitation anomaly for month 2 of the forecasts during June–September 1987 from ensemble mean and superensemble, respectively. The ensemble mean of the models showed a negative anomaly over northeastern India and a positive anomaly over the rest of the Indian region. This pattern of the spatial distribution of anomaly was opposite of that observed in the IMD datasets (Fig. 8a). The anomaly correlation (indicated inside the panel) was −0.64 for the ensemble mean forecasts. The superensemble successfully forecasted the observed positive anomaly over northeastern India and a negative anomaly over central and south India during this year. The anomaly correlation from the superensemble was 0.33. During 1988 (Figs. 8e,f), the ensemble mean of the member models predicted a slightly negative anomaly over south India and a positive anomaly over eastern and northern India. This pattern was opposite to that observed (Fig. 8d). During this year, the superensemble performed slightly better than the ensemble mean in predicting the spatial pattern of precipitation anomaly over the Indian region. The signature of positive anomaly over south India and patches of the positive and negative anomaly over eastern India is present in the superensemble datasets. However, note that the predicted anomaly by the superensemble was very low compared to the observation.

Another set of years with an opposite precipitation anomaly during our study period was 1994 and 2000. During 1994, area-averaged precipitation over the Indian region exceeded 24.4% (9.8%) of its 1987–2001 climatology during July (June–September) in the CMAP data. The corresponding increase in the IMD dataset was 16.5% (7.0%). On the other hand, during the

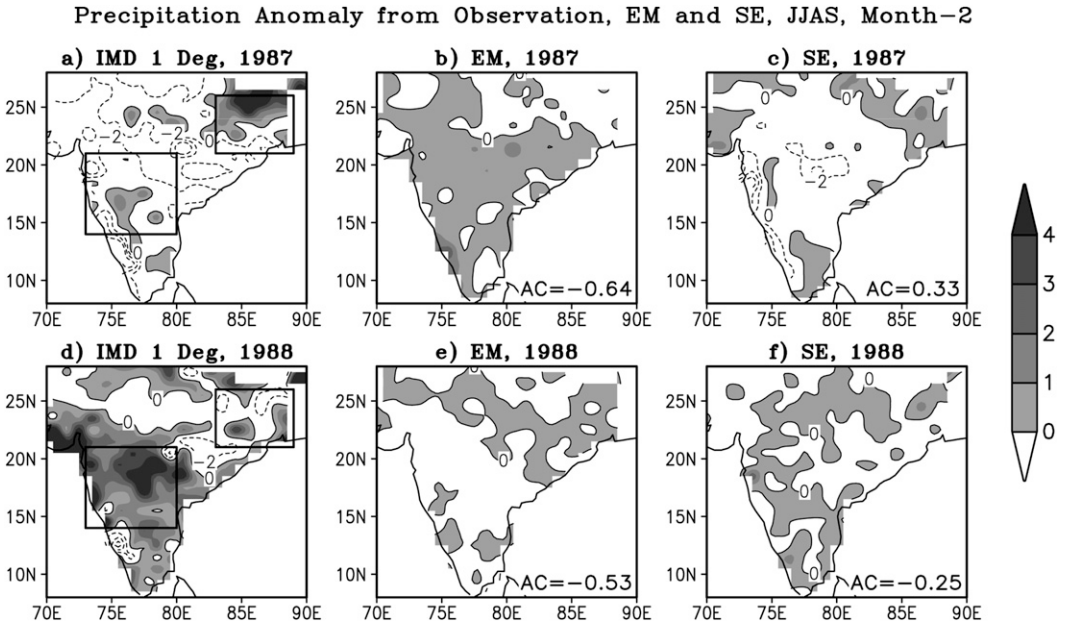

FIG. 8. Precipitation anomaly during June–September 1987 (dry year) and 1988 (wet year) from IMD observation, the ensemble mean, and superensemble forecasts. The anomaly correlation (AC) for the forecasted fields are indicated. (a),(d) Two regions shown are used for analysis in Figs. 10a,b.

monsoon season of 2000, the mean precipitation was lower than normal by 7.0% (12.7%) during July (June–September) in the CMAP dataset. The IMD dataset shows the negative anomaly as 8.2% (11.6%) during July (June–September). The observed and forecasted precipitation during June–September during these two years over the Indian region is shown in Fig. 9. However, as can be seen from Figs. 9a,c, the precipitation anomaly was not of the same sign all over the Indian region during either of these years. During 1994, northern and southwestern India experienced heavier-than-normal precipitation. In the contrary, precipitation over south-central and southeastern India was below normal. The situation was almost opposite during 2000. In this year, northern India experienced less-than-normal precipitation, whereas the precipitation anomaly was positive in the south Indian peninsula. The forecasted precipitation anomaly during these two years from the ensemble mean and superensemble are shown in Figs. 9b,c and in Figs. 9e,f, respectively. The ensemble mean of the models could not forecast the observed positive (negative) anomaly in north (south) India during 1994. The anomaly correlation for this forecast was −0.56. The signature of the north–south dipole in the precipitation anomaly was forecasted reasonably by the superensemble (Fig. 9c) in this year (AC = 0.09). During June–September 2000, the ensemble mean of the models showed a positive anomaly almost over the entire Indian region (AC = −0.48). However, forecasted precipitation from the superensemble showed a negative anomaly over north India and a negative anomaly over south India (AC = 0.28), which is consistent with the observation.

The skills of the ensemble mean and the superensemble during 1987, 1988, 1994, and 2000 are further examined in Fig. 10. Figures 10a,b show the averaged precipitation anomaly during 1987 and 1988 over the two boxes indicated in Figs. 8a,d from IMD-based observations and forecasts from the ensemble mean and the superensemble. The method of area averaging was a simple mean of the anomaly values of the grid points weighted by their area, which is dependent on the latitude. Over south-central India (14°–21°N, 73°–80°E, Fig. 10a), the negative anomaly of precipitation exceeded 1 mm day^{-1} in the observation during 1987. This was reasonably predicted by the superensemble. The ensemble mean showed a slight positive anomaly during this year over this region. During 1988 over the same region an anomaly of observed precipitation was positive (>2 mm day^{-1}). Neither the ensemble mean nor the superensemble was able to predict this positive anomaly reasonably (the anomaly was negative in the ensemble mean datasets). Over northeastern India (21°–26°N, 83°–89°E, Fig. 10b) the situation was opposite. During 1987, the observed positive anomaly exceeded 0.5 mm day^{-1}. The ensemble mean showed a negative anomaly during this year. The superensemble was able to predict this sign of anomaly successfully. During 1988,

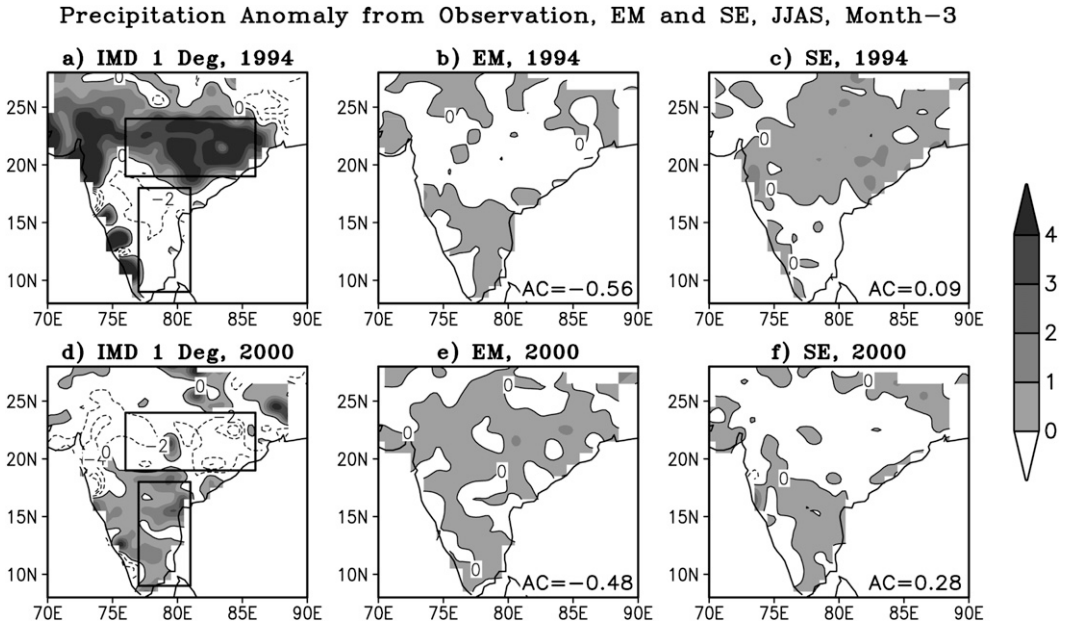

FIG. 9. As in Fig. 8, but for June–September 1994 (wet year) and 2000 (dry year).

the observed anomaly over this region was negative (~ -0.2 mm day^{-1}). The ensemble mean showed a positive anomaly during this year. It was possible to reasonably forecast the sign and magnitude of the observed anomaly of precipitation over this region during 1988 by the downscaled superensemble.

Figures 10c,d show the precipitation anomaly over the two boxes indicated in Figs. 9a,d during June–September 1994 and 2000 from observation and model forecasts. These two regions were chosen to best represent the observed seesaw in the dipole of precipitation anomaly over north and south India during these two years. During 1994 over southern India (9°–18°N, 77°–81°E) observed precipitation was below normal by more than 1.5 mm day^{-1}. The ensemble mean showed a slight positive signature and the superensemble showed a slight negative signature in the precipitation anomaly over this region in 1994. The observed anomaly was positive during 2000 over this region. The superensemble showed a slight positive anomaly in this year, which was consistent with the observation. Over the northern Indian region (19°–24°N, 76°–86°E), observed precipitation was way above normal (by about 4 mm day^{-1}) during 1994, and below normal (by about 2 mm day^{-1}) during 2000 (Fig. 10d). The ensemble mean forecast showed a negative anomaly over this region during 1994 and a positive anomaly during 2000. The precipitation anomaly from the superensemble was of the same sign of that of the IMD observation during these two years, although the magnitude of the anomalies were much less. An analysis of ETS results during these two years reveals that (not shown) the superensemble appears promising to forecast heavier precipitation over the Indian region.

f. Forecast skills as a function of domain size for downscaling

The question of seasonal rainfall forecasts improvements, regionally as against ''all India,'' has been an important unsolved problem (Gadgil and Kumar 2006). Having noted a marked improvement of the seasonal ETS over all-India from downscaled superensemble we ask the pertinent question about the regional skills by examining a successive sequence of smaller and smaller subdomains. These are arbitrarily selected to cover the following domains (Fig. 11, right panel): A (8°–28°N, 70°–90°E), B (10°–25°N, 70°–85°E), C (10°–20°N, 73°–83°E), D (10°–15°N, 75°–80°E), and E (20°–23°N, 75°–78°E). A comparison of month 2 of forecasts for July from the ensemble mean and the superensemble with the observed IMD rains are presented in Fig. 12. Here we present the precipitation totals separately over the selected five regions during July 1987–2001. The correlation and RMS error of forecasted time series with the observation are indicated inside the respective panels. The rainfall totals of the member models is reflected in the ensemble mean that shows a general degradation in the seasonal rainfall forecast as the domain of evaluation is reduced in size. However, the most striking result here is that there is much less degradation of results as a function of the domain size from the downscaled multimodel superensemble. This is a promising result for the future possibilities for regional prediction

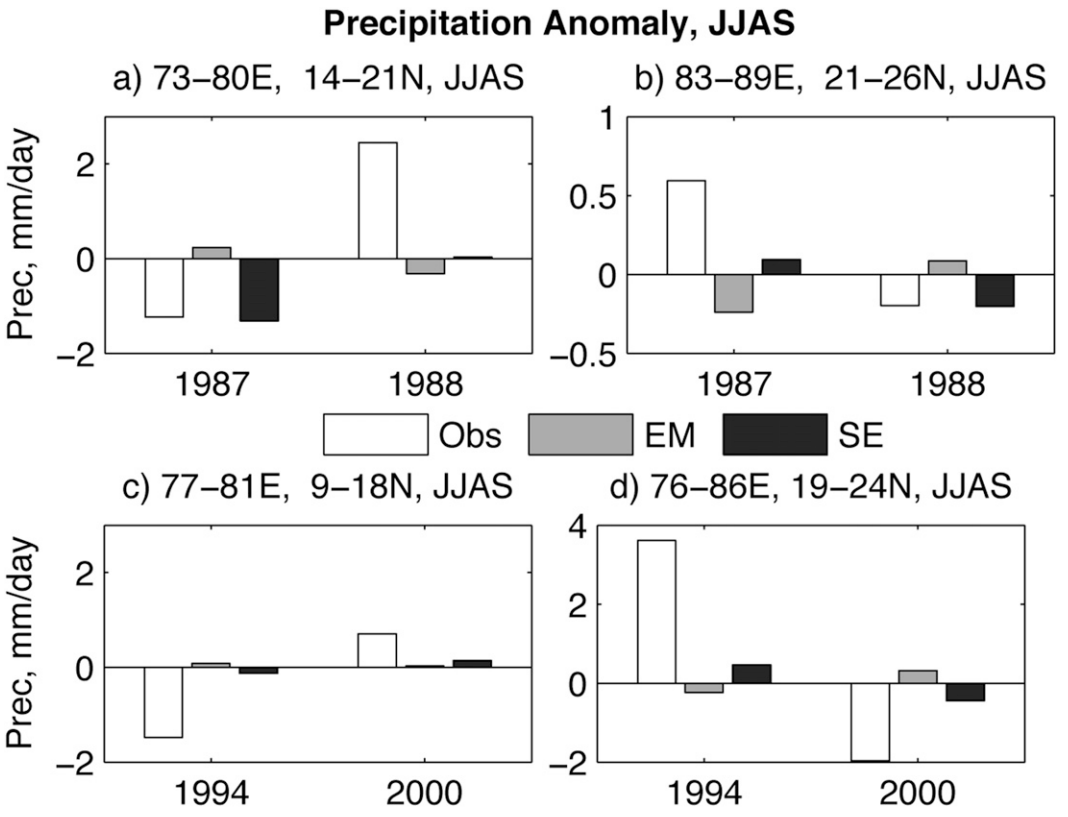

FIG. 10. Precipitation anomaly during June–September (a) 1987 (dry year), (b) 1988 (wet year), (c) 1994 (wet year), and (d) 2000 (dry year) over the subregions shown in Figs. 8 and 9 from the IMD observation (Obs), the ensemble mean (EM), and the superensemble (SE) forecasts.

of seasonal rainfall from the use of downscaling and the superensemble algorithm.

g. Ranked probability skill score

The ranked probability skill score (RPSS) measures forecast skill relative to the climatology. RPSS is defined as (Hamill et al. 2004)

$$\mathrm{RPSS} = 1 - \frac{\mathrm{RPS}}{\mathrm{RPS}_{\mathrm{ref}}}, \tag{12}$$

where RPS and $\mathrm{RPS}_{\mathrm{ref}}$ are ranked probability scores (RPS) of the actual forecast and a reference forecast, respectively. In this study, we have taken the reference forecast as the climatology. RPS is defined as

$$\mathrm{RPS} = \frac{1}{M-1}\sum_{m=1}^{M}\left(\sum_{k=1}^{m} p_k - \sum_{k=1}^{m} o_k\right)^2, \tag{13}$$

where M is the number of different forecast categories or bins (e.g., 0.0–0.5, 0.5–1.0, …, 49.5–50.0 mm day^{-1}), p_k is the forecasted probability in category k, and o_k equals 1 (0) if the observation falls (does not fall) into category k. RPS measures the skill of an ensemble forecast to be within the category of the observation. Valid values of RPS vary from 0 to 1, with 0 signifying perfect skill and 1 signifying no skill. If there are N number of models in an ensemble ($N = 4$ for this study) then the expression for p_k can be written as

$$p_k = \sum_{i=1}^{N} w_i \delta(F_i), \tag{14}$$

where w_i is weight for the ith model, F_i is forecast from the ith model, and $\delta(F_i)$ is a delta function given by

$$\delta(F_i) = \begin{cases} 1, & \text{if} \quad F_i \in k; \\ 0, & \text{otherwise.} \end{cases} \tag{15}$$

The value of w_i equals $1/N$ for a simple ensemble forecast that relies equally on every model.

Although the superensemble provides the deterministic forecast, it was shown by Stefanova and Krishnamurti (2002) that the superensemble carries an equivalent probabilistic forecast as well. The expression for the superensemble forecast [Eq. (5)] can be rewritten as

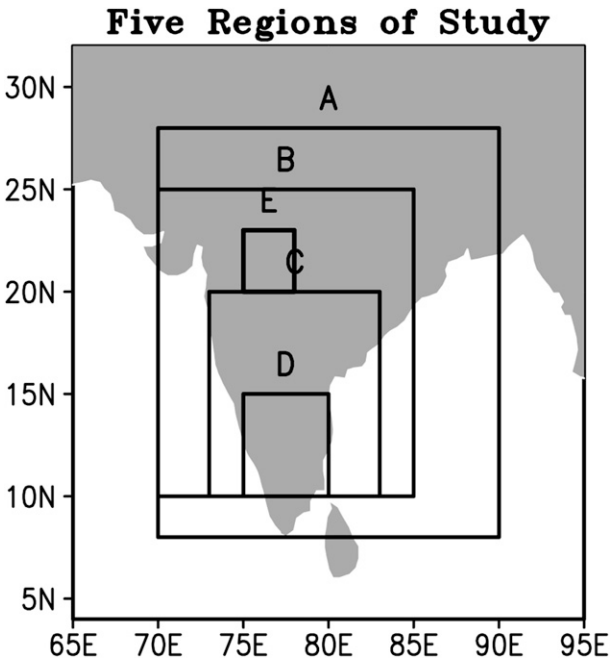

FIG. 11. Five subdomains of Fig. 12.

$$S = \frac{1}{N}\sum_{i=1}^{N}[Na_i(F_i - \overline{F}_i) + \overline{O}] = \frac{1}{N}\sum_{i=1}^{N} S_{pi}, \tag{16}$$

where S_{pi} can be considered as modified forecast from the ith model. Equation (16) is equivalent to simple ensemble forecast from a suite of multimodels:

$$E = \frac{1}{N}\sum_{i=1}^{N} F_i. \tag{17}$$

However, to assign probability to the modified model forecasts S_{pi} for the superensemble, one should take into account the fact that the superensemble does not rely equally on every model. The model that performs better in the training period should get a higher weight for calculating probability. To assign weights to different models for probabilistic forecast by the superensemble, we have adopted the strategy described in Stefanova and Krishnamurti (2002). This method normalizes the weights of the individual models used to calculate the superensemble forecast [a_is of Eq. (5)]:

$$w_i = \frac{\sqrt{|a_i|}}{\sum_{i=1}^{N}\sqrt{|a_i|}}, \tag{18}$$

where w_i is the weight used to calculate RPS and N is the number of models. The square root was taken following the study of Stefanova and Krishnamurti (2002), which shows that this provides a better probabilistic forecast compared to a the case when the degree of a_i is 1. To calculate p_k for the superensemble, we first calculated modified model forecasts S_{pi} according to Eq. (16). If S_{pi} falls into category k, then the probability p_k for that category was increased by w_i. This exercise was repeated for modified forecasts from all the four FSU models before calculating RPS using Eq. (13).

We have considered bin sizes of 0.5 mm day^{-1} to calculate RPSS for downscaled precipitation forecasts from the four member ensemble and the superensemble. The results for July 1987 (a month when precipitation over the Indian region was 32% below normal) from the simple ensemble forecast and the superensemble forecast is shown in Figs. 13a,b, respectively. In this figure, grids with RPSS values less than 0 (i.e., those that indicate no skill relative to the climatology) were not shaded. The higher the value of RPSS, the better the skill of forecast over the climatology (RPSS = 1 signifies 100% skill or a perfect forecast). Note that there were more grids in the simple ensemble forecast compared to the superensemble where the forecast skill did not exceed the skill of climatology. During this month, 12.2% more grids in the superensemble showed forecast skill better than the climatology (RPSS $>$ 0) when compared to the simple ensemble. Moreover, forecasts from the superensemble showed higher skills (higher RPSS) over most of the grids compared to the simple ensemble forecasts.

Figure 13c shows the difference in the number of grids over the domain 8°–28°N, 70°–90°E between the simple ensemble and the superensemble forecasts where forecast skill exceeded that of the climatology. Note that, during most of the months in this 15-yr period, the RPSS value exceeded the zero value over more grid points from the superensemble forecasts compared to the simple ensemble forecasts. During June–September 1987, 1988, 1994, and 2000 (the extreme monsoon years discussed in section 7e), 7.7%, 4.2%, 9.4%, and 10.4% more grids, respectively, exceeded the skill of the climatology over the Indian region when the superensemble is used compared to the simple ensemble forecasts.

8. Concluding remarks and future work

The present study became possible because of the availability of a very dense rain gauge network over India. The availability of roughly 2100 rain gauge–based rainfall estimates on a daily basis made it possible to use these on 1.0° × 1.0° resolution for downscaling and the superensemble methodology. The coupled global

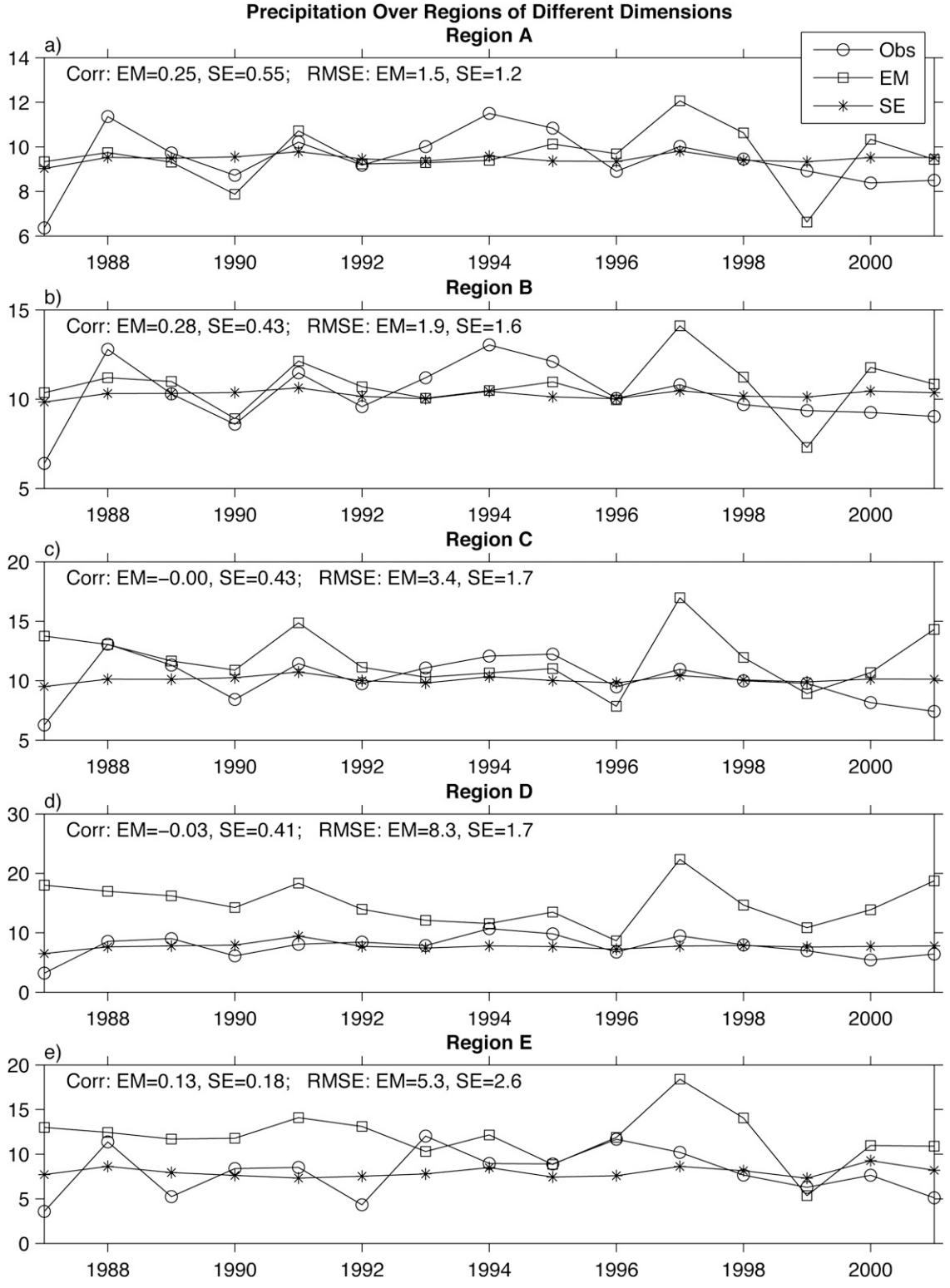

FIG. 12. Precipitation over five subdomains (shown in Fig. 11) from the observation, the ensemble mean, and the superensemble during July 1987–2001. The correlation and RMS errors between the observed and forecasted time series are indicated at the top.

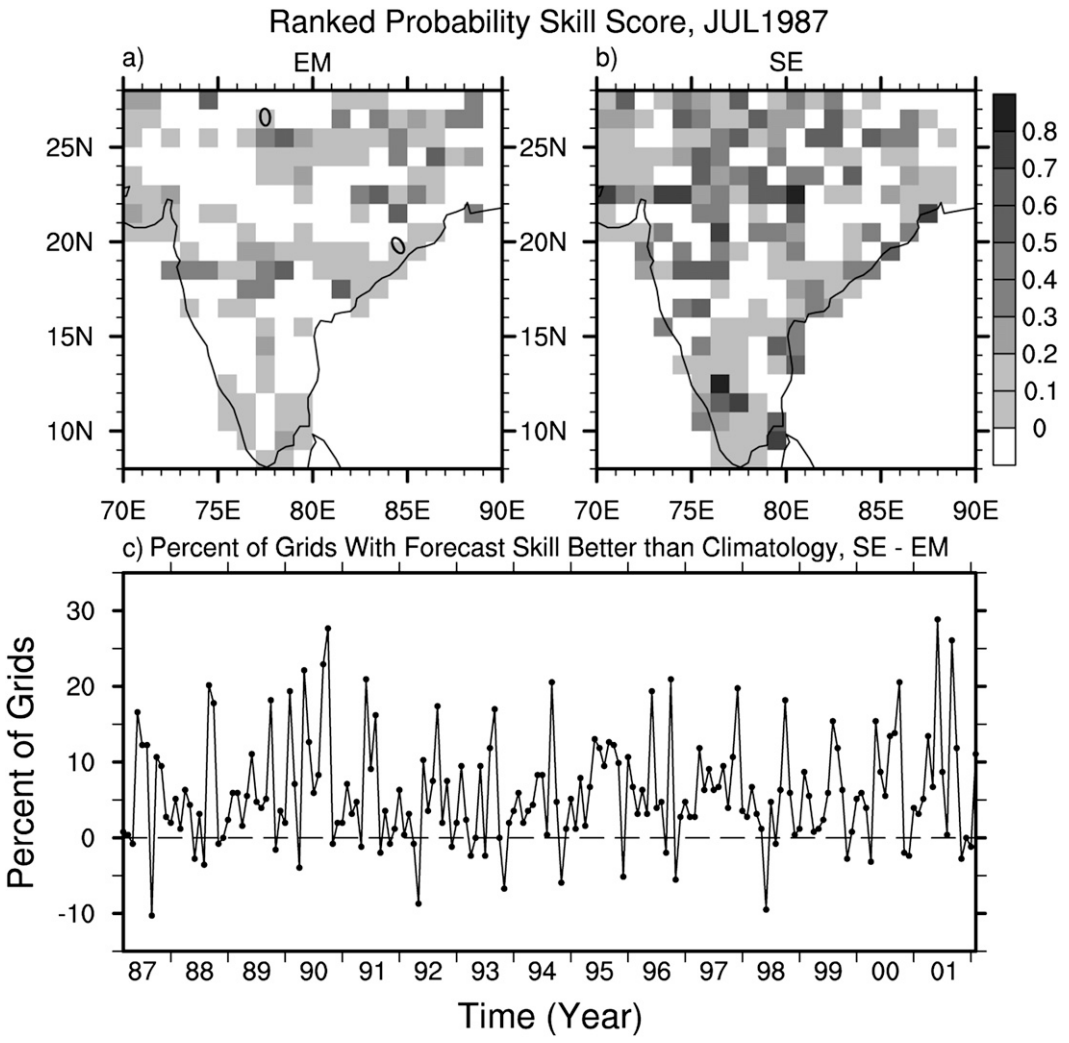

FIG. 13. RPSS of month-3 precipitation forecasts for July 1987 from (a) the ensemble mean and (b) the superensemble. RPSS ≤ 0.0 signifies no skill compared to climatology. A skill of 1.0 shows a perfect forecast. (c) The difference in the percent of grids between the ensemble mean and the superensemble over the domain 8°–28°N, 70°–90°E those show higher skill than climatology for month 3 of forecasts.

modeling for the prediction of seasonal climate, presented in this study, is an extension of our previous studies (Krishnamurti et al. 2006a,b; Chakraborty and Krishnamurti 2006). The present study includes a downscaling counterpart. Each of the models forecasts of precipitation is subjected to a statistical downscaling. The coefficients of our downscaling equation were based on 14 yr of training datasets. It was shown that these coefficients assume a stable value when number of years in the training phase crosses 10. However, one of the coefficients [viz., b of Eq. (2)] did not get a high degree of stability even with 14 yr of training. This could have introduced some error in the results presented in this paper. However, after looking at Fig. 5 we feel that this error will not be high since the fluctuation of the value of b decreased substantially when the number of years in the training phase crossed 7. The downscaling exercise showed that each of the member models climatology for the seasonal rains (after the downscaling) achieved very high skills ($\sim$0.98 for this pattern correlation), this compares with scores $\sim$0.5 prior to downscaling. The downscaled product for each of the member models was next used for the construction of the multimodel superensemble for the monthly and seasonal forecasts of rains. A major impact of the downscaling was noted for each member model's seasonal rain. We further noted that the superensemble of the downscaled member models improved the results for rainfall prediction when compared to results from downscaled single models as well as the downscaled ensemble mean.

A measure of the level of improvement for the seasonal precipitation forecasts is illustrated in Fig. 7. We can see a vast improvement on the 1.0° × 1.0° latitude–longitude resolution. In Fig. 1 we have seen that the coarse-resolution (CMAP) and higher-resolution (IMD) observed precipitation datasets are somewhat different in their spatial patterns. This difference between the two observed datasets can have some consequences when coarse-resolution and downscaled model results are intercompared. However, it is shown in the manuscript that we get a huge improvement in the forecast skill with the proposed downscaling methodology compared to the coarse-resolution models. Therefore, it can be said that the results presented in this manuscript are robust and the improvement of forecast skill due to downscaling is not dependent on the quality of the observed datasets.

The downscaling algorithm for each member model corrects the slope and intercept of the rainfall history of each model based on the training period. The slope is a measure of the rate of increase of model rains as compared to those of the observations. The intercept error is an overall systematic underestimation or overestimation of the model rains. These errors were corrected by our downscaling algorithm. The use of multimodel superensembles on these downscaled model precipitation estimates further improves the skill of the forecast compared to the individual models or their ensemble mean.

Although in this study we used only 15 yr of datasets, there were 6 yr during this period when the precipitation over the Indian region was far from normal. This includes four extreme years [viz., 1987 (below normal), 1988 (above normal), 1994 (above normal), and 2000 (below normal)]. We have shown, in this manuscript that during these 4 yr the skill of the downscaled superensemble was better than the corresponding ensemble mean forecast.

One of the limitations of this downscaling strategy could be that it cannot capture the dynamically varying relationship between the model output and observation that can arise due to climate change. We plan to extend our methodology in the future to be able to capture the observed changes in the value of the parameters being downscaled.

Recently, a huge rain gauge–based precipitation database is being compiled under the Asian Precipitation Highly Resolved Observational Data Integration towards Evaluation of Water Resources (APHRODITE) project (Xie et al. 2007). This covers nearly 50 yr of daily rainfall datasets. This covers the regions of the Asian summer monsoon, the Middle East, and Africa. It would be possible to expand the downscaling and the multimodel superensemble forecasts of seasonal climate to cover this entire domain. It would also be possible to carry out the downscaling and the construction of the superensemble using a site-specific (instead of grid point based) downscaling and superensemble constructions. Thus, these rain gauge sites would replace the grid points. This approach calls for the interpolation of the model output rains from their spectral transform grid locations to these rain gauge locations, thereafter, the entire downscaling and the superensemble would be carried out at the rain gauge sites. This is worth exploring in the context of seasonal climate forecasts at high resolution.

REFERENCES

Anandhi, A., V. V. Srinivas, R. S. Nanjundiah, and D. N. Kumar, 2008: Downscaling precipitation to a river basin in India for IPCC SRES scenarios using the support vector machine. *Int. J. Climatol.,* **28,** 401–420.

Anthes, R. A., 1977: A cumulus parameterization scheme utilizing a one-dimensional cloud model. *Mon. Wea. Rev.,* **105,** 270–286.

Arakawa, A., and W. H. Schubert, 1974: Interaction of a cumulus cloud ensemble with the large-scale environment, Part I. *J. Atmos. Sci.,* **31,** 674–701.

Brankovic, C., and T. N. Palmer, 1997: Atmospheric seasonal predictability and estimates of ensemble size. *Mon. Wea. Rev.,* **125,** 859–874.

——, ——, F. Molenti, S. Tibaldi, and U. Cubasch, 1990: Extended range predictions with ECMWF models: Time lagged ensemble forecasting. *Quart. J. Roy. Meteor. Soc.,* **116,** 867–912.

Chakraborty, A., and T. N. Krishnamurti, 2006: Improved seasonal climate forecasts of the south Asian summer monsoon using a suite of 13 coupled ocean–atmosphere models. *Mon. Wea. Rev.,* **134,** 1697–1721.

——, ——, and C. Gnanaseelan, 2007: Prediction of the diurnal cycle using a multimodel superensemble. Part II: Clouds. *Mon. Wea. Rev.,* **135,** 4097–4116.

Chang, C. P., Ed., 2004: *East Asian Monsoon.* World Scientific, 564 pp.

——, and T. N. Krishnamurti, Eds., 1987: *Monsoon Meteorology*. Oxford University Press, 560 pp.

——, B. Wang, and N.-C. G. Lau, 2005: The global monsoon system: Research and forecast. World Meteorological Organization, WMO/TD 1266, 28 pp.

Déqué, M., 1997: Ensemble size for numerical seasonal forecasts. *Tellus,* **49A,** 74–78.

Gadgil, S., and K. R. Kumar, 2006: Agriculture and economy. *The Asian Monsoon,* B. Wang, Ed., Springer-Verlag, 203–257.

Gowariker, V., V. Thapliyal, S. M. Kulshrestha, G. S. Mandal, N. Sen Roy, and D. R. Sikka, 1991: A power regression model for long range forecast of southwest monsoon rainfall over India. *Mausam,* **42,** 125–130.

Grell, G. A., 1993: Prognostic evaluation of assumptions used by cumulus parameterization. *Mon. Wea. Rev.,* **121,** 764–787.

Hamill, T. M., J. S. Whitaker, and X. Wei, 2004: Ensemble reforecasting: Improving medium-range forecast skill using retrospective forecasts. *Mon. Wea. Rev.,* **132,** 1434–1447.

Ji, Y., and A. D. Vernekar, 1997: Simulation of the Asian summer monsoons of 1987 and 1988 with a regional model nested in a global GCM. *J. Climate,* **10,** 1965–1979.

Krishnamurti, T. N., and H. S. Bedi, 1988: Cumulus parameterization and rainfall rates: Part III. *Mon. Wea. Rev.,* **116,** 583–599.

——, and J. Sanjay, 2003: A new approach to the cumulus parameterization issue. *Tellus,* **55,** 275–300.

——, Y. Ramanathan, H. L. Pan, R. J. Pasch, and J. Molinary, 1980: Cumulus parameterization and rainfall rates: Part I. *Mon. Wea. Rev.,* **108,** 465–472.

——, J. Xue, H. S. Bedi, K. Ingles, and D. Oosterhof, 1991: Physical initialization for numerical weather prediction over the tropics. *Tellus,* **43,** 53–81.

——, C. M. Kishtawal, T. E. LaRow, D. R. Bachiochi, Z. Zhang, C. E. Williford, S. Gadgil, and S. Surendran, 1999: Improved weather and seasonal climate forecasts from multimodel superensemble. *Science,* **285,** 1548–1550.

——, D. Bachiochi, T. LaRow, B. Jha, M. Tewari, D. Chakraborty, R. Correa-Torres, and D. Oosterhof, 2000a: Coupled atmosphere–ocean modeling of the El Niño of 1997–98. *J. Climate,* **13,** 2428–2459.

——, C. M. Kishtawal, Z. Zhang, T. E. LaRow, D. R. Bachiochi, C. E. Williford, S. Gadgil, and S. Surendran, 2000b: Multimodel superensemble forecasts for weather and seasonal climate. *J. Climate,* **13,** 4196–4216.

——, L. Stefanova, A. Chakraborty, T. S. V. V. Kumar, S. Cocke, D. Bachiochi, and B. Mackey, 2002: Seasonal forecasts of precipitation anomalies for North American and Asian monsoons. *J. Meteor. Soc. Japan,* **80,** 1415–1426.

——, A. Chakraborty, R. Krishnamurti, W. K. Dewar, and C. A. Clayson, 2006a: Seasonal prediction of sea surface temperature anomalies using a suite of 13 coupled atmosphere–ocean models. *J. Climate,* **19,** 6069–6088.

——, A. K. Mitra, W.-T. Yun, and T. S. V. V. Kumar, 2006b: Seasonal climate forecasts of the Asian monsoon using multiple coupled models. *Tellus,* **58A,** 487–507.

——, A. K. Mishra, A. Chakraborty, and M. Rajeevan, 2009: Improving global model precipitation forecasts over India using downscaling and the FSU superensemble. Part I: 1–5-day forecasts. *Mon. Wea. Rev.,* **137,** 2713–2735.

Kumar, K. K., M. Hoerling, and B. Rajagopalan, 2005: Advancing dynamical prediction of Indian monsoon rainfall. *Geophys. Res. Lett.,* **32,** L08704, doi:10.1029/2004GL021979.

Kummerow, C., W. Barnes, T. Kozu, J. Shiue, and J. Simpson, 1998: The Tropical Rainfall Measuring Mission (TRMM) sensor package. *J. Atmos. Oceanic Technol.,* **15,** 809–817.

Larow, T. E., and T. N. Krishnamurti, 1998: Initial conditions and ENSO prediction using a coupled ocean-atmosphere model. *Tellus,* **50,** 76–94.

Misra, V., and M. Kanamitsu, 2004: Anomaly nesting: A methodology to downscale seasonal climate simulations from AGCMs. *J. Climate,* **17,** 3249–3262.

Palmer, T. N., and Coauthors, 2004: Development of a European Multimodel Ensemble System for Seasonal to Interannual Prediction (DEMETER). *Bull. Amer. Meteor. Soc.,* **85,** 853–872.

Peng, P., A. Kumar, A. H. van den Dool, and A. G. Barnston, 2002: An analysis of multimodel ensemble predictions for seasonal climate anomalies. *J. Geophys. Res.,* **107,** 4710, doi:10.1029/2002JD002712.

Rajagopalan, B., U. Lall, and S. Zebiak, 2002: Categorical climate forecasts through regularization and optimal combination of multiple GCM ensembles. *Mon. Wea. Rev.,* **130,** 1792–1811.

Rajeevan, M., D. S. Pai, S. K. Dikshit, and R. R. Kelkar, 2004: IMD's new operational models for long-range forecast of southwest monsoon rainfall over India and their verification for 2003. *Curr. Sci.,* **86,** 422–431.

——, J. Bhate, J. Kale, and B. Lal, 2006: High resolution daily gridded rainfall data for the Indian region: Analysis of break and active monsoon spells. *Curr. Sci.,* **91,** 296–306.

Regonda, S. K., B. Rajagopalan, and M. Clark, 2006: A new method to produce categorical streamflow forecasts. *Water Resour. Res.,* **42,** W09501, doi:10.1029/2006WR004984.

Reynolds, R. W., and T. M. Smith, 1994: Improved global sea surface temperature analysis using optimum interpolation. *J. Climate,* **7,** 929–948.

Rogers, E., T. Black, D. Deaven, G. DiMego, Q. Zhao, M. Baldwin, N. Junker, and Y. Lin, 1996: Changes to the operational early ETA analysis/forecast system at the National Centers for Environmental Prediction. *Wea. Forecasting,* **11,** 391–413.

Shepard, D., 1968: A two-dimensional interpolation function for irregularly spaced data. *Proc. 1968 ACM National Conf.,* Princeton, NJ, ACM, 517–524.

Sperber, K. R., and T. N. Palmer, 1996: Interannual tropical rainfall variability in general circulation model simulations associated with the Atmospheric Model Intercomparison Project. *J. Climate,* **9,** 2727–2750.

Stefanova, L., and T. N. Krishnamurti, 2002: Interpretation of seasonal climate forecast using Brier skill score, FSU superensemble, and the AMIP-I dataset. *J. Climate,* **15,** 537–544.

Stephenson, D. B., C. A. S. Coelho, F. J. Doblas-Reyes, and M. Balmaseda, 2005: Forecast assimilation: A unified framework for the combination of multi-model weather and climate predictions. *Tellus,* **57,** 253–264.

Thapliyal, V., and S. M. Kulshrestha, 1992: Recent models for long-range forecasting of south–west monsoon rainfall over India. *Mausam,* **43,** 239–248.

Tripathi, S., V. V. Srinivas, and R. S. Nanjundiah, 2006: Downscaling of precipitation for climate change scenarios: A support vector machine approach. *J. Hydrol.,* **330,** 621–640.

Vernekar, A. D., and Y. Ji, 1999: Simulation of the onset and intraseasonal variability of two contrasting summer monsoons. *J. Climate,* **12,** 1707–1725.

Walker, G. T., 1923: Correlation in seasonal variations of weather. VIII: A preliminary study of world weather. IMD Memo. XXIII, Part IV, 75–131.

——, 1924: Correlation in seasonal variations of weather. IX: A further study of world weather. IMD Memo. XXIV, Part IX, 75–131.

Wang, B., Ed., 2006: *The Asian Monsoon*. Springer-Verlag, 844 pp.

——, Q. Ding, X. Fu, I.-S. Kang, K. Jin, J. Shukla, and F. Doblas-Reyes, 2005: Fundamental challenge in simulation and prediction of summer monsoon rainfall. *Geophys. Res. Lett.,* **32,** L15711, doi:10.1029/2005Gl022734.

Wolff, J.-O., E. Maier-Reimer, and S. Legutke, 1997: The Hamburg Ocean Primitive Equation Model HOPE. DKRZ Tech. Rep. 13, Modellberatungsgruppe, 98 pp.

Xie, P., and P. A. Arkin, 1997: A 17-year monthly analysis based on gauge observations, satellite estimates, and numerical model outputs. *Bull. Amer. Meteor. Soc.,* **78,** 2539–2558.

——, M. Chen, S. Yang, A. Yatagai, T. Hayasaka, Y. Fukushima, and C. Liu, 2007: A gauge-based analysis of daily precipitation over East Asia. *J. Hydrometeor.,* **8,** 607–626.

Yang, X.-Q., and J. L. Anderson, 2000: Correction of systematic errors in coupled GCM forecasts. *J. Climate,* **13,** 2072–2085.

Yun, W.-T., L. Stefanova, A. K. Mitra, T. S. V. V. Kumar, W. Dewar, and T. N. Krishnamurti, 2005: Multimodel synthetic superensemble algorithm for seasonal climate prediction using DEMETER forecasts. *Tellus,* **57,** 280–289.